Observed Relationships between Electric Fields and Auroral Particle Precipitation

D. A. GURNETT AND L. A. FRANK

Department of Physics and Astronomy, University of Iowa
Iowa City, Iowa 52240

Simultaneous electric field and plasma observations with the low-altitude polar-orbiting satellite Injun 5 have provided a comprehensive survey of convection electric fields and their association with magnetospheric plasma phenomena. The most prominent features of the convection electric fields are reversals located at high magnetic latitudes, with generally antisunward convection poleward and sunward convection equatorward of the electric field reversal location. The electric field reversal is interpreted as the boundary between open and closed magnetic field lines. During local day the electric field reversal is observed to coincide with the equatorward boundary of the polar cusp. The plasma flow in the dayside polar cusp region is dominantly E-W, away from the stagnation point, the convection velocities typically being $\sim$1 km sec^{-1}. At local evening, 'inverted V' electron precipitation bands are observed near or at the position of the electric field reversal. In the local late-evening sector the electric field reversal becomes less distinct, and often no single well-defined electric field reversal can be identified. In all cases the inverted V electron precipitation events are closely associated with large, typically $>$30 mv m^{-1}, irregular electric field fluctuations with time scales of a few seconds or less. Often these fluctuations comprise distinct 'spikes' of a few seconds duration or less, which can be identified with distinct boundaries or other features of the electron precipitation. In the local midnight sector, convection electric fields of $>$50 mv m^{-1} associated with plasma sheet electrons have been observed extending deep into the magnetosphere, equatorward of the electron ($E > 45$ kev) trapping boundary. These convection electric fields are characterized by considerably smaller fluctuations relative to those observed within the inverted V electron precipitation bands. To investigate the electric field and plasma interrelationships during a polar magnetic substorm, a series of passes obtained before and during a substorm is presented. Large antisunward convection velocities were detected over the polar cap several tens of minutes before the onset of the expansive phase of the substorm. These convection velocities gradually decreased during the decay phase of the substorm. Our measurements of enhanced antisunward flow over the polar cap region are generally consistent with several current ideas concerning the origin of substorms.

Electric field measurements with satellites [*Cauffman and Gurnett*, 1971; *Heppner*, 1972] and ionized barium cloud releases [*Haerendel and Lust*, 1970; *Wescott et al.*, 1969] have now established the primary features of magnetospheric plasma convection at low altitudes over the auroral zones and polar caps (see, for example, the reviews by *Cauffman and Gurnett* [1972] and *Haerendel* [1971]). Similarly, extensive measurements of low-energy auroral charged particles have also been acquired (see the review by *Hultqvist* [1969]), and a comprehensive spatial survey of the energy spectra and intensities of auroral charged particles has been presented by *Frank and Ackerson* [1972].

However, until recently, only a few simultaneous measurements of convection electric fields and auroral particle precipitation have been available for studying the relationship between these phenomena.

In a previous paper [*Frank and Gurnett*, 1971] an initial investigation of electric fields and charged-particle observations was presented with data from the low-altitude satellite Injun 5 for orbits passing through the dawn-dusk local time sectors. This initial study revealed several important relationships between convection electric fields and the charged-particle intensities. In particular, the 'trapping boundary' for electrons with energies of $\gtrsim$45 kev was found to be coincident with a reversal in the E-W direction of the plasma flow com-

monly observed in the high-latitude convection pattern, and intense 'inverted V' electron precipitation bands of the type reported by *Frank and Ackerson* [1971] were observed at or poleward of the trapping boundary. This paper presents a detailed study of the relationship between electric fields and the auroral charged-particle precipitation, particularly on the dayside of the magnetosphere and in the region of the intense inverted V electron precipitation bands, which most frequently constitute the primary auroral particle precipitation in the local afternoon and evening sectors. These latter observations will use the substantial telemetry capability of Injun 5 to make simultaneous high time resolution measurements of electric fields and auroral particle precipitation. A series of electric field and plasma observations obtained during a polar magnetic substorm is also analyzed to provide further information on the dynamical behavior of the magnetosphere during magnetic disturbances.

INSTRUMENTATION

Injun 5 was launched on August 8, 1968, into a near-polar orbit with an apogee of 2528 km and a perigee of 677 km. The electric field sensors on Injun 5 comprise two conducting spheres mounted on booms with a center-to-center separation of 2.85 meters. The spacecraft is oriented by a bar magnet within the spacecraft such that the electric antenna axis is always maintained approximately perpendicular to the local geomagnetic field vector. The electric field component parallel to the electric antenna axis is determined by measuring the potential difference between the spheres with a high-impedance voltmeter. (See *Gurnett et al.* [1969] for a complete description of the electric field instrumentation on Injun 5.) To determine the convection electric field in the plasma, the $\mathbf{V}_s \times \mathbf{B}$ electric field caused by the spacecraft motion through the ionosphere and small instrumental errors must be subtracted from the measured electric field. Since only a single-axis electric antenna is used, it is to be emphasized that only one component of the convection electric field (or convection velocity) can be determined. Generally, the accuracy of the convection electric field determination is limited to approximately ± 30 mv m^{-1} by errors due to asymmetrical sunlight shadowing of the spheres by the supporting booms. However, for certain orientations and when the spacecraft is rotating very slowly, the accuracy of the electric field determination is much better, approximately ± 10 mv m^{-1} or less (see discussions by *Cauffman and Gurnett* [1971]). Except where it is noted, all the electric field data presented in this paper are selected for conditions when the convection electric field can be determined to an accuracy of ± 10 mv m^{-1} or better.

Simultaneous measurements of electron and proton intensities within the energy range of $5 \leq E \leq 50{,}000$ ev are provided by two low-energy proton and electron differential energy analyzers. These two electrostatic analyzers provide simultaneous measurements of the differential energy spectrums of proton and electron intensities within fields of view centered at pitch angles $\alpha = 0°$ and $\alpha = 90°$. Directional intensities of more energetic ($E > 45$ kev) electrons are measured with a companion set of thin-windowed Geiger-Mueller tubes. The spacecraft carries a tape recorder with a bit rate of 800 bits sec^{-1} for worldwide spatial surveys and has a high bit rate mode of operation at 24,000 bits sec^{-1} for high temporal resolution studies. Further description of the satellite and its charged-particle instrumentation is given by *Frank and Ackerson* [1971].

POLAR CUSP OBSERVATIONS

From the observations of *Frank* [1971*a*] it is known that plasma from the dayside magnetosheath has direct access into the high-latitude magnetosphere through a region called the polar cusp. To illustrate the general relationship between the charged-particle intensities and convection electric fields in the polar cusp region, three polar passes have been selected for presentation. These passes were selected entirely on the basis of the quality of the electric field observations and without reference to the related charged-particle intensities, so that no known bias is present in the charged-particle–electric field relationships shown. In each case it was required that the accuracy of the electric field determination be better than ± 10 mv m^{-1} and that a clearly defined electric field reversal, representative of the high-latitude electric fields observed with Injun 5, be detectable.

Figure 1 illustrates a meridional pass through the high-latitude dayside magnetosphere in the

local early afternoon sector. The polar cusp region is easily identified in this case by the enhanced intensities of low-energy electrons ($105 \leq E \leq 185$ ev) and protons ($290 \leq E \leq 455$ ev) at 08h 50m 10s to 08h 52m 10s UT. From the intensities of electrons with energies $E > 45$ kev at pitch angles $\alpha = 90°$ it is seen that the polar cusp is located just poleward of the electron ($E > 45$ kev) trapping boundary. The trapping boundary is observationally identified with the high-latitude termination of measurable, $\sim 5 \times 10^1$ el (cm^2 sec ster)$^{-1}$, $E >$ 45-kev electron intensities. The relationship between the electron ($E > 45$ kev) trapping boundary and the polar cusp illustrated in Figure 1 is typical of the polar cusp observations previously reported by *Frank and Ackerson* [1971, 1972]. The polar cusp identification in this case is further supported by the simultaneous occurrence of broad band VLF hiss in the polar cusp. *Gurnett and Frank* [1972] have demonstrated that broad band VLF hiss of the type shown in Figure 1 is associated with the relatively intense fluxes, $dJ/dE \gtrsim 10^4$–10^5 (cm^2 sec ster ev)$^{-1}$, of low-energy ($\sim$100 ev) electrons in the polar cusp.

The electric field measurements for this pass are also shown in Figure 1. The convection electric field component along the antenna axis E_c is given by the difference between the measured electric field and the $\mathbf{V}_s \times \mathbf{B}$ field component along the antenna axis. Because of the slow rotation rate of the spacecraft and the absence of sunlight shadowing errors the convection electric field can be determined with exceptionally good accuracy, $\sim$5 mv m^{-1}, during this pass. A clearly defined electric field reversal is evident at 08h 50m 10s UT, coincident with the electron ($E > 45$ kev) trapping boundary and with the equatorward boundary of the polar cusp within the temporal resolution of these survey measurements. The spacecraft orientation near the reversal region is such that the electric antenna is measuring the N-S component of the convection electric field. The corresponding directions for the plasma convection velocity components are shown in the magnetic local time versus invariant latitude polar diagram of Figure 2. The arrows in Figure 2 are in the directions of the convection velocity component detected, and the length of the arrows is proportional to the magnitude of the convection velocity computed

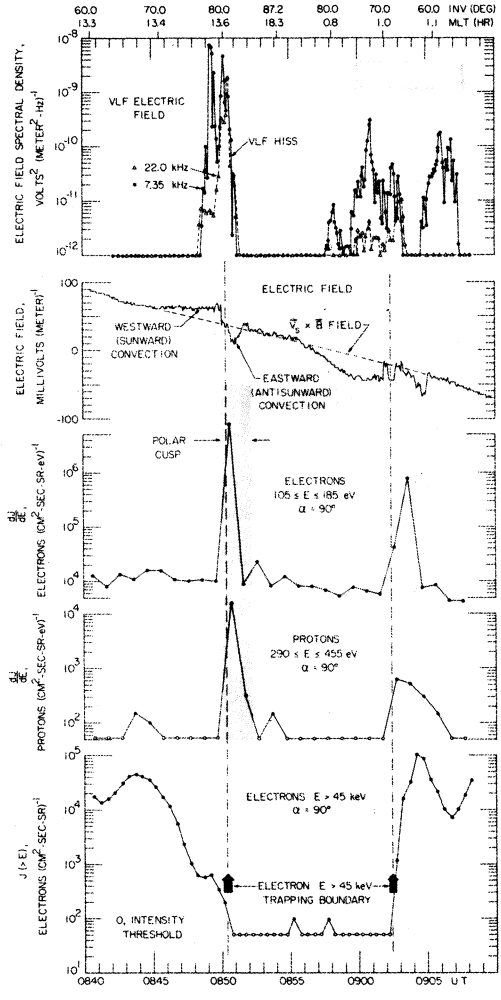

Fig. 1. Simultaneous observations of VLF hiss, convection electric fields, and charged-particle intensities for a noon-midnight meridional pass (orbit 7476, April 15, 1970) over the southern polar cap and auroral zone. Note that the polar cusp (shaded area) is located in the zone of eastward convection just poleward of the electric field reversal and the electron ($E > 45$ kev) trapping boundary. The width of the solid black arrow indicates the range of uncertainty in determining the trapping boundary locations. The measured electric field (solid line) and the $\mathbf{V}_c \times \mathbf{B}$ field component along the antenna axis (horizontal dashed line) are indicated.

from $V_c = E_c/B$, where E_c is the magnitude of the convection electric field component detected and B is the scalar value of the local geomagnetic field. Note that the arrows in Figure 2 do not represent the vector direction of the plasma

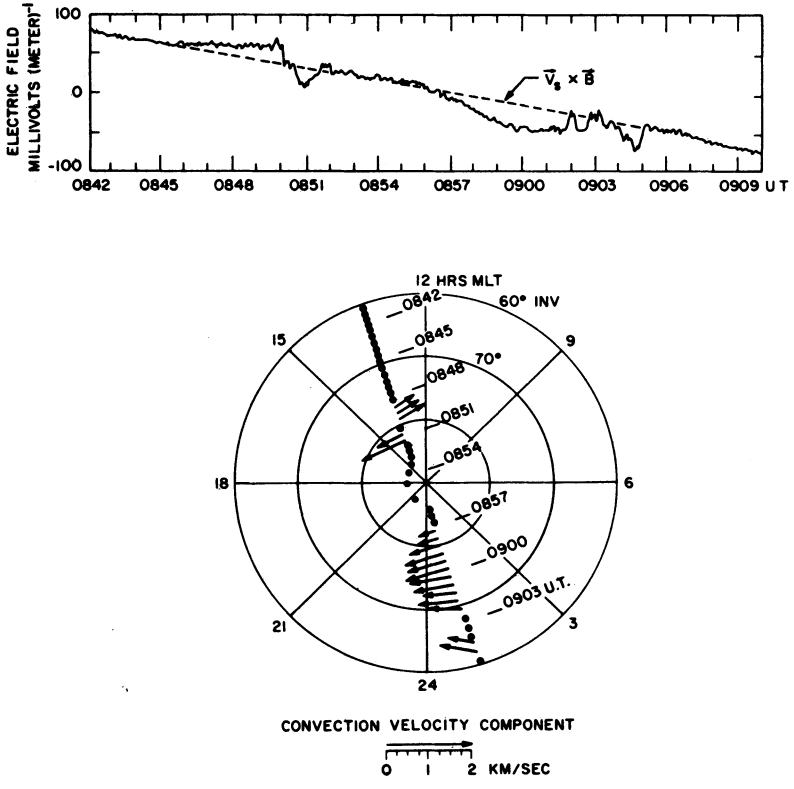

Fig. 2. A polar diagram showing the direction and magnitude of the convection velocity components associated with the electric field observations in Figure 1. The polar cusp is located within the zone of eastward convection at 08h 50m 10s to 08h 52m 10s UT.

convection, since only one component of the convection electric field (hence convection velocity) is measured. The negative electric field component of about 25 mv m^{-1} at 0851 UT, poleward of the electric field reversal, corresponds to the eastward convection velocity component of about 1 km sec^{-1}. Equatorward of the electric field reversal the convection is westward. Note from Figure 1 that, although the maximum low-energy electron and proton intensities occur very near the electric field reversal, measurable proton intensities associated with the polar cusp are observed throughout the region of eastward convection poleward of the reversal. Over the polar cap, at about 08h 52m 00s to 08h 57m 00s UT, no convection electric fields greater than about 10 mv m^{-1} are detectable. In the postmidnight sector a large region of westward convection is observed extending from 08h 57m 00s to 09h 05m 00s UT.

Figure 3 shows two additional polar passes selected to further demonstrate the relationship between convection electric fields and charged-particle intensities in the polar cusp. The first pass, orbit 7561, is very close to the local noon meridian. The polar cusp is identified again by the dramatic enhancement of intensities of low-energy protons with energies of $290 \leq E \leq 455$ and $1030 \leq E \leq 1610$ ev and electrons with energies of $400 \leq E \leq 705$ ev at 08h 30m 00s to 08h 32m 00s UT. The magnetic local time at the time of passage through the polar cusp is about 12.4 hours. The low-energy electron intensities in the polar cusp occur in a narrow latitudinal band, $\sim 2°$ wide, adjacent to and poleward of the electron ($E > 45$ kev) trapping boundary. The low-energy proton intensities are present in a somewhat broader latitudinal band, $\sim 3°$ wide, which extends slightly poleward of the low-energy electron precipitation region. The characteristic soft energy spectrum of the polar cusp protons is evident in Figure 3 from

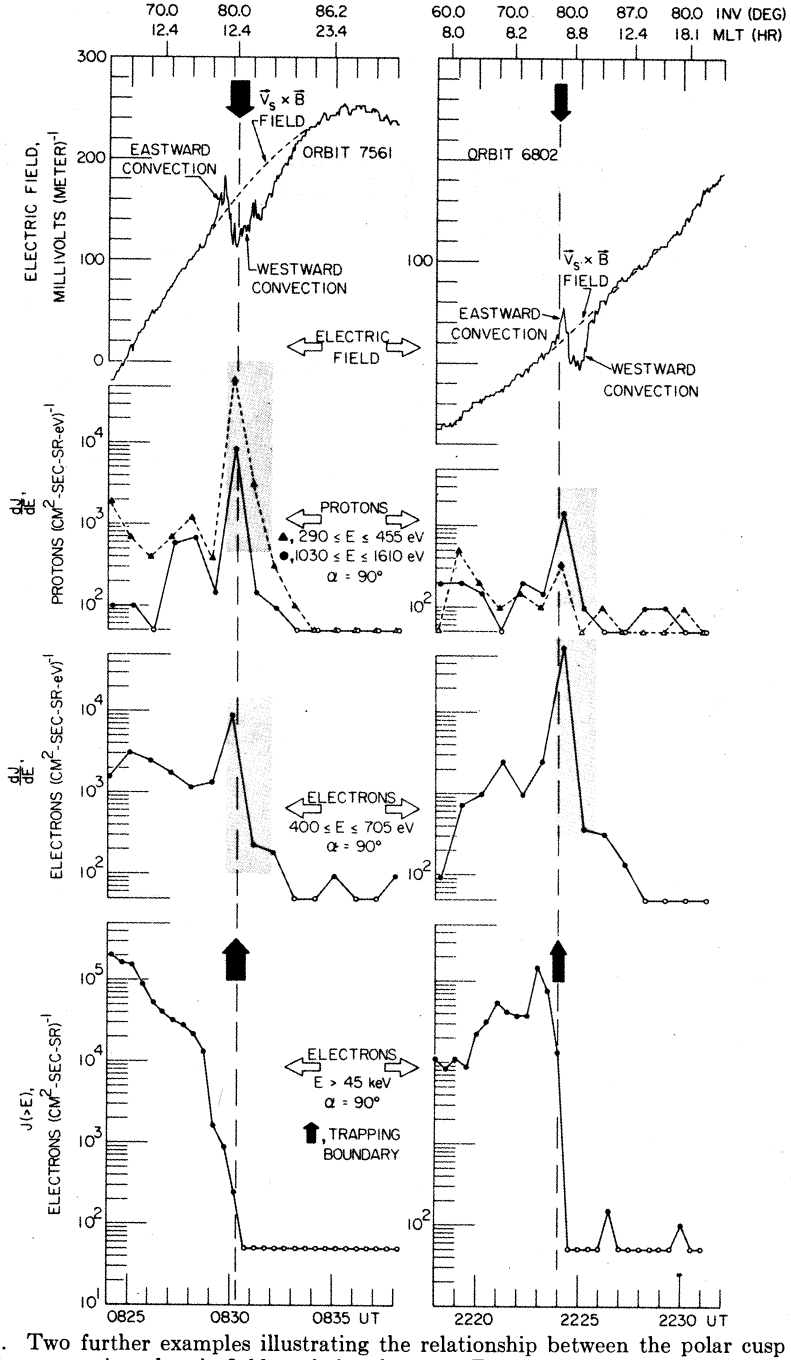

Fig. 3. Two further examples illustrating the relationship between the polar cusp (shaded area), the convection electric field, and the electron ($E > 45$ kev) trapping boundary (vertical dashed lines). Orbit 7561 (April 22, 1970) is over the southern hemisphere, and orbit 6802 (February 18, 1970) is over the northern hemisphere.

the relative intensities of $290 \leq E \leq 455$ and $1030 \leq E \leq 1610$ ev protons.

The electric field for orbit 7561 has a clearly defined reversal located at 08h 30m 00s UT. From Figure 3 it is seen that this electric field reversal is coincident with the location of the electron ($E > 45$ kev) trapping boundary within the temporal resolution of these survey measurements. The magnetic local time versus invariant latitude polar diagram for the convection velocity components associated with this electric field reversal is shown in Figure 4. Equatorward of the electric field reversal a small zone of eastward convection is observed in a region of substantial electron ($E > 45$ kev) intensities at $\alpha = 90°$. Poleward of the electric field reversal there is a larger zone of generally westward plasma convection in a region void of electron ($E > 45$ kev) intensities. The polar cusp plasma is located within this region of westward plasma convection just poleward of the electric field reversal and the electron ($E > 45$ kev) trapping boundary. At higher latitudes the convection velocity component decreases until it is essentially zero over the polar cap at 08h 33m 00s to 08h 40m 00s UT. It is important to note that the orientation of the electric field antenna changes by more than 90°

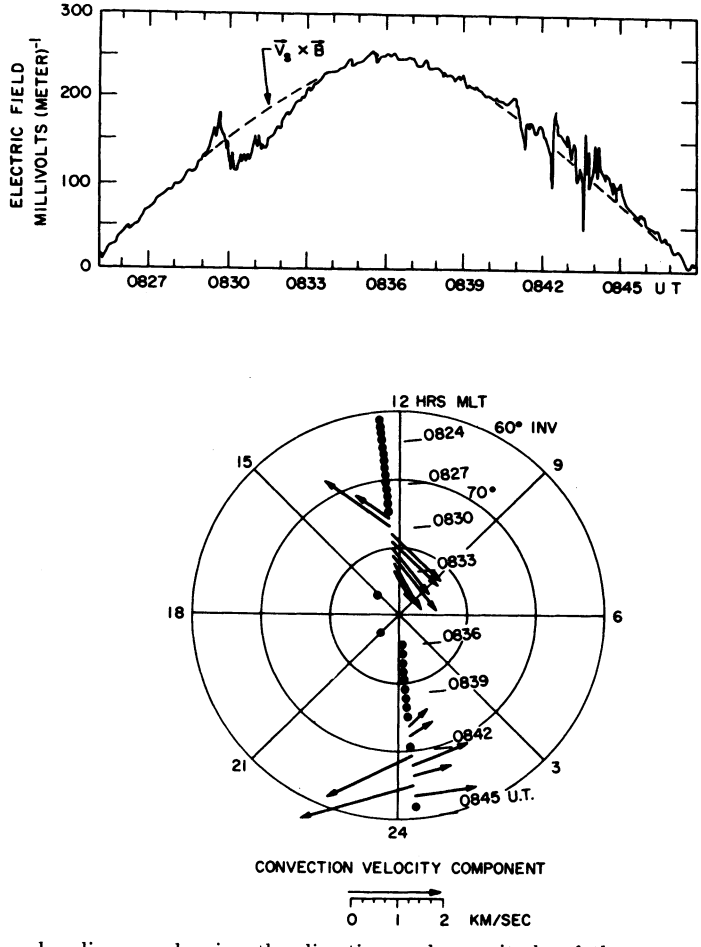

Fig. 4. A polar diagram showing the direction and magnitude of the convection velocity components for the southern hemisphere polar pass of orbit 7561 in Figure 3. The convection velocity in the polar cusp, from about 0830 to 0832 UT, is westward, and thus it is indicated that the 'stagnation point' for the polar cusp plasma flow is located east of the spacecraft for this example.

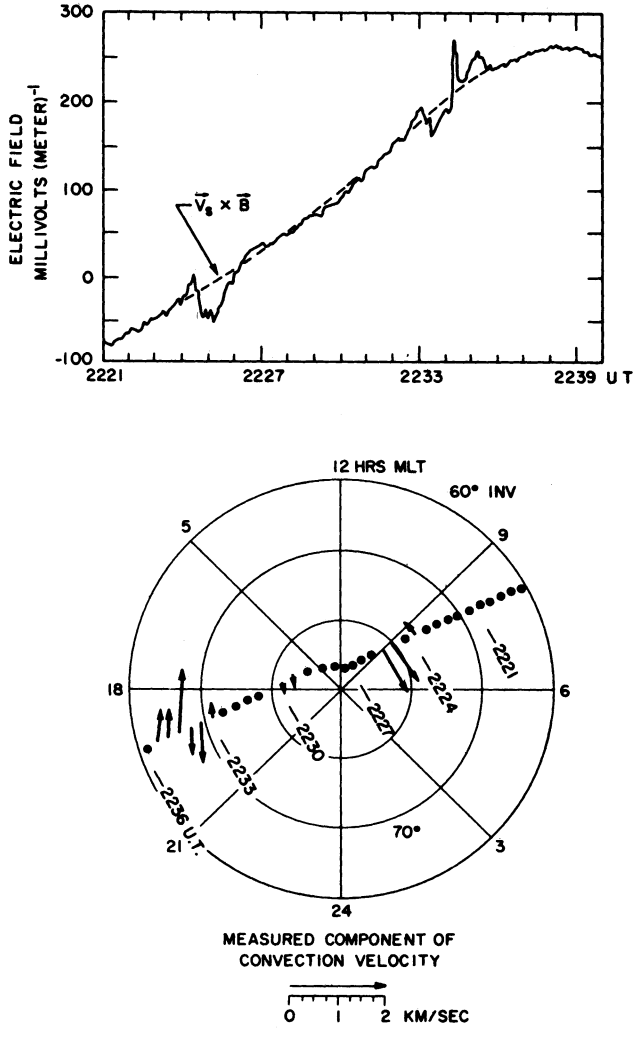

Fig. 5. A polar diagram showing the direction and magnitude of the convection velocity components for the northern hemisphere polar pass of orbit 6802 in Figure 3. The maximum low-energy electron intensities in the polar cusp are encountered essentially coincident with the electric field reversal at 22h 24m 20s UT.

over the polar cap, so that any convection electric field greater than about 10 mv m^{-1} should have been detected.

The second pass, orbit 6802, shown in Figure 3 is selected as an example of a polar cusp observation in the local morning sector at ~9.0 hours MLT. Here the polar cusp location is best identified by the increase in the low-energy electron intensities. The low-energy proton intensities observed in the polar cusp region during this pass are seen to be much lower than those of the two cases discussed above. The reduced low-energy proton intensities at this local time are typical of polar cusp observations at local times more than about 3 hours from local noon [*Frank and Ackerson*, 1972]. The low-energy electron intensities in the polar cusp are again positioned in a narrow latitudinal band, about 3° wide, poleward of and adjacent to the electron ($E > 45$ kev) trapping boundary.

The convection electric field observed on orbit 6802 has a clearly defined reversal located at 22h 24m 20s UT. From Figure 3 it is seen that

the electric field reversal is again coincident with the electron ($E > 45$ kev) trapping boundary and the maximum polar cusp electron and proton intensities. The convection velocity components associated with this electric field reversal are shown in the magnetic local time versus invariant latitude polar diagram of Figure 5. Equatorward of the electric field reversal a zone of eastward (sunward) convection is observed. This zone of sunward convection is within the region of measurable intensities of mirroring electrons ($E > 45$ kev) equatorward of the trapping boundary. Poleward of the electric field reversal a larger zone of westward (antisunward) plasma convection is observed. This westward convection zone extends 1° or 2° in latitude poleward of the detectable polar cusp plasma. Because of the low intensities of the polar cusp protons relative to those of the local noon sector it is difficult to determine accurately the poleward extent of the polar cusp plasma at this local time solely from charged-particle measurements.

Discussion and Interpretation of the Polar Cusp Observations

As is shown by *Cauffman and Gurnett* [1972], the plasma convection in the dayside high-latitude auroral zone is primarily E-W and comprises a poleward zone and an equatorward zone separated by an electric field reversal. The E-W directions of the plasma convection are opposite in these two zones. Except in the region within about ±2 hours of local noon the E-W convection component is generally away from the sun in the poleward zone and toward the sun in the equatorward zone. The convection zones are generally only a few degrees wide in latitude near local noon, but they increase considerably in width toward local evening and morning. In some cases the region of antisunward convection can expand over the entire polar region with relatively uniform antisunward convection velocities from dawn to dusk. In most cases, however, the antisunward convection is relatively nonuniform, the maximum convection velocities occurring in the region just poleward of the electric field reversal, particularly in the local dawn sector of the auroral zone [e.g., *Cauffman and Gurnett*, 1971, Figure 7]. The observed plasma convection pattern is broadly consistent with the flow pattern expected in the magnetospheric model recently proposed by us [*Frank*, 1971*a*, *b*; *Frank and Gurnett*, 1971], which employs *Dungey*'s [1961] concept of merging of geomagnetic field lines with the interplanetary magnetic field to provide access of magnetosheath plasma to the magnetospheric interior. In this interpretation the electric field reversal occurs on magnetic field lines that connect with the merging region, the antisunward flow poleward of the electric field reversal is on 'open' magnetic field lines that connect into the magnetosheath and solar wind, and the sunward flow equatorward of the electric field reversal corresponds to the return flow of 'closed' magnetic field lines within the magnetosphere. Within about ±2 hours of local noon the E-W sense of the flow at low altitudes is not persistently the same on successive passes at a given magnetic local time, presumably owing to the variations in the position of the distant neutral point at the magnetopause and the angle of attack of the solar wind.

The plasma convection observations shown in Figures 2, 4, and 5 provide an excellent illustration of the convection pattern generally found on the dayside of the magnetosphere. The convection directions near the reversal at 08h 50m 10s UT in Figure 2 are characteristic of the dusk convection cell with eastward convection on the poleward side of the reversal and a westward return flow on the equatorward side of the reversal, as would be expected at this local time (~13.6 hours MLT). The convection directions observed for the reversal at 08h 30m 00s UT in Figure 4, very close to local noon, are the opposite of those shown in Figure 2, indicating that this plasma convection is associated with the dawn convection cell. Other observations near local noon [*Cauffman and Gurnett*, 1972] demonstrate that both eastward and westward convection velocities occur with about equal probabilities in this region. The convection directions for the electric field reversal at 22h 24m 20s UT in Figure 5 are characteristic of the dawn convection cell, as would be expected at this local time (~8.7 hours MLT).

The polar cusp observations shown in Figures 2 and 5, together with the examples previously published by *Gurnett and Frank* [1972], provide a remarkably consistent picture of the association between convection electric fields

and the polar cusp plasma. These measurements show that in all cases the electric field reversal is coincident, to within the accuracy of the determination, with the electron ($E > 45$ kev) trapping boundary. The low-energy polar cusp protons with energies of several hundreds of electron volts are found to occur in a narrow latitudinal band, typically about 2° wide, located just poleward of the electron ($E > 45$ kev) trapping boundary and extending into the region of antisunward flow poleward of the electric field reversal. It should be noted that without the full range of diagnostic capabilities available from Injun 5 it would be difficult to clearly determine the latitudinal width of the polar cusp region with the low-energy plasma observations alone. For example, for orbit 7561 of Figure 3 the low-energy ($1030 \leq E \leq 1610$ ev) proton intensities are significantly above the background levels at 08h 27m 00s to 08h 32m 00s UT. Both the convection electric field and the electron ($E > 45$ kev) measurements, however, provide compelling evidence that the protons at 08h 27m 00s to 08h 30m 00s UT are on closed field lines within the magnetosphere and cannot be identified as polar cusp plasma. The relatively hard energy spectrum of the protons compared with the soft energy spectrum of the polar cusp protons, evident in Figure 2, adds further confirming evidence of the proper identification of these two plasma regimes. Difficulties in distinguishing between these two plasma regimes because of limited diagnostic capabilities are believed to account for the large widths (~5°) of the polar cusp observations by *Heikkila and Winningham* [1971] compared with the typical polar cusp widths (~2°) obtained from Injun 5 [see also *Frank and Ackerson*, 1972].

The low-energy (~100 ev) polar cusp electrons are observed in a narrow latitudinal band, typically $\lesssim 2°$ wide, located within the low-energy proton band, the peak intensities usually being near the equatorward boundary. A relatively rare example for which the polar cusp plasma is separated into a distinct equatorward 'electron sheet' and a poleward 'proton sheet,' as is more often observed in the distant polar cusp [*Frank*, 1971*a*], is given by *Gurnett and Frank* [1972, Figure 1]. At the low altitudes of Injun 5, however, the electron band is usually embedded within the proton band as it is in Figures 1 and 3. Typically, the maximum intensities of low-energy polar cusp electrons are observed to be coincident with the electron ($E > 45$ kev) trapping boundary and the electric field reversal.

Since the low-energy protons in the polar cusp are identified as the signature of the direct entry of magnetosheath plasma to low altitudes, these observations show that the region of generally antisunward plasma convection (away from the stagnation point) poleward of the electric field reversal is on open magnetic field lines that connect into the magnetosheath and solar wind. The presence of measurable intensities of mirroring electrons with energies $\gtrsim 45$ kev equatorward of the electric field reversal lends considerable support to the interpretation that this region of generally sunward plasma convection (toward the dayside magnetopause) is on closed magnetic field lines. The intense fluxes of low-energy (~100 ev to 1 kev) electrons often observed at the electric field reversal are believed to result from electron acceleration and heating in the merging region.

Observations of Auroral Precipitation in the Local Evening

Frank and Ackerson [1972] have found that, when the low-energy electron precipitation band observed in the polar cusp is followed around into the local evening, the average energy of the precipitated electrons increases to several kev or more. These electron precipitation bands are observed to have a characteristic inverted V energy-time signature, the average electron energy increasing to a maximum and subsequently decreasing as the spacecraft passes through the precipitation region [*Frank and Ackerson*, 1971]. During periods of relative magnetic quiescence, these inverted V events provide the primary charged-particle energy input into the auroral zone in the local afternoon and evening and have been directly associated with visible auroral arcs [*Ackerson and Frank*, 1972].

To determine the relationship between the inverted V electron precipitation events and convection electron fields, we have examined the observations from about 50 passes over the auroral zone at local afternoon and evening. Because the duration of the inverted V events is often only a few tens of seconds or less, only measurements acquired via the high bit rate

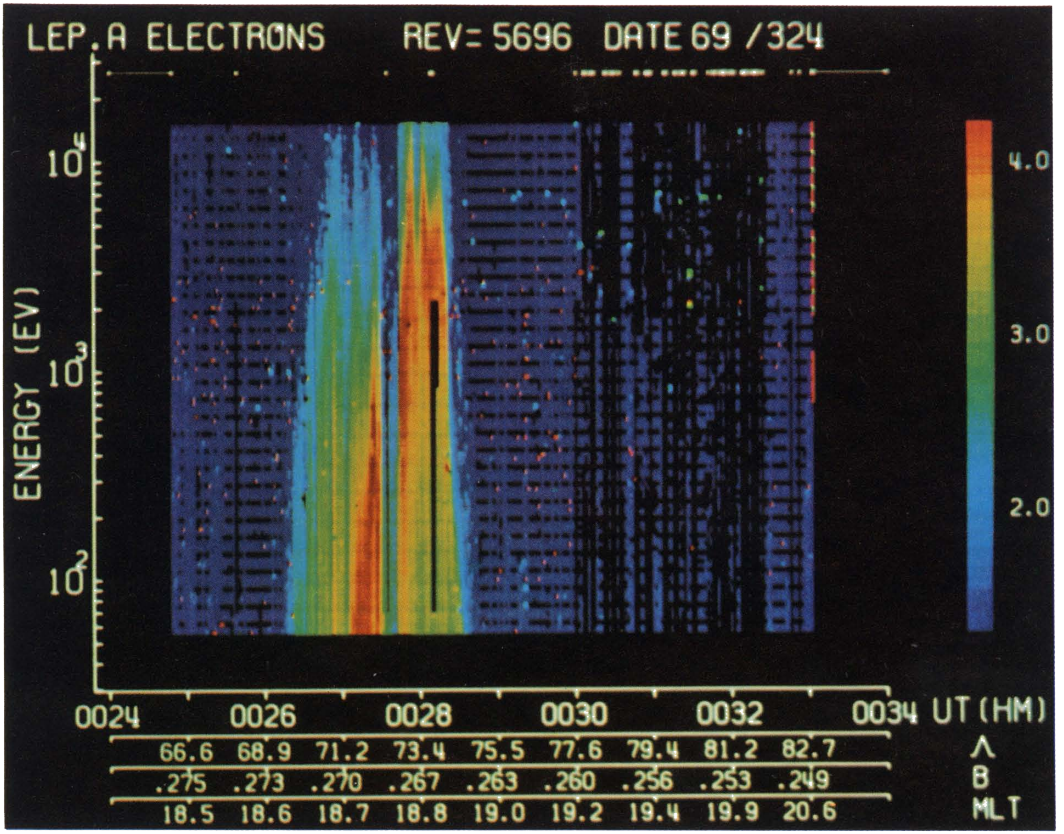

Plate 1. Energy-time spectrogram of the precipitated electron intensities observed for a northern hemisphere pass over the auroral zone at about 18.8 hours MLT. Several distinct inverted V electron precipitation events are observed at 00h 27m 10s to 00h 28m 20s UT.

mode of operation were used in this part of the study. Since the telemetry station viewing range for high bit rate acquisition is greatest when the satellite position attains its highest altitudes, most of this telemetry was obtained at relatively high altitudes ($\gtrsim$1500 km). Because the electron densities at high altitudes are often too low for satisfactory operation of the electric field experiment, the selection of high bit rate telemetry suitable for comparisons of the electric field and charged particles was correspondingly limited. Essentially no auroral zone measurements obtained at altitudes above about 1800 km during local winter could be used because of the substantial levels of electric field noise commonly detected in this region [*Cauffman and Gurnett*, 1971]. Only measurements within regions where the electron densities are greater than about 10^3 el cm^{-3} were considered satisfactory for the electric field determinations in this study. Most of the observations examined here were obtained over the northern hemisphere during the summer of 1969.

From the cases studied a series of four passes has been selected to illustrate relationships that were either commonly observed or otherwise of special interest, as will be noted. The spacecraft orientation and the rotation rate in each of these cases are such that the electric field can be determined with excellent accuracy, <10 mv m^{-1}, with no possibility of spurious effects such as errors due to sunlight shadowing of the spheres or wake effects. No attempt was made to select these passes on the basis of magnetic activity, although in no case does the Kp index exceed 3. The passes are discussed in the order of increasing local time.

Orbit 5696. The first pass selected for pre-

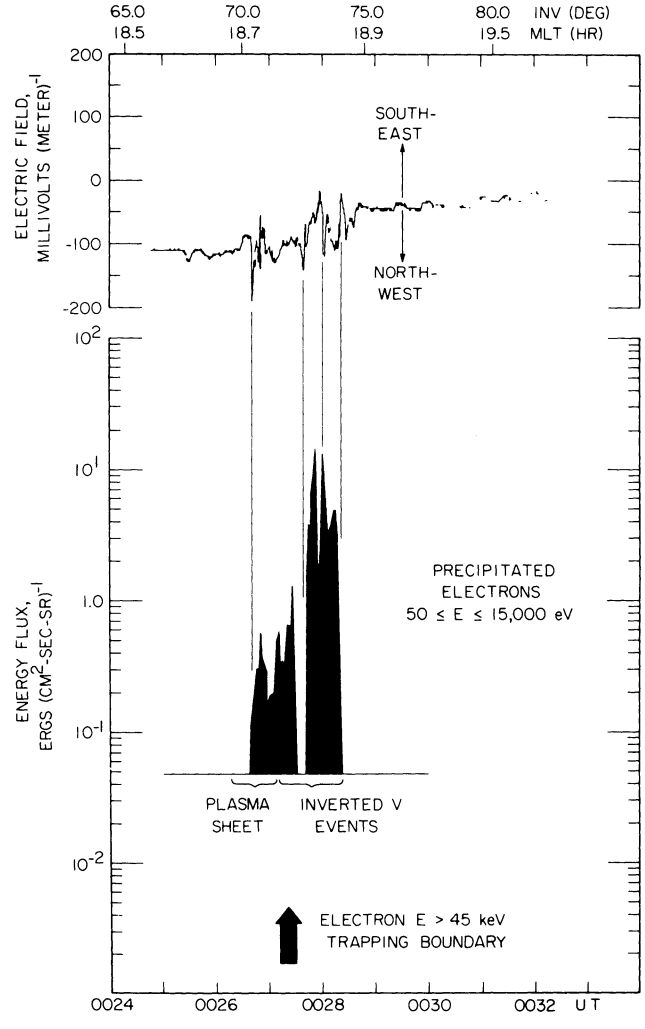

Fig. 6. The electric field and precipitated electron energy fluxes corresponding to the energy-time spectrogram of Plate 1 for orbit 5696 over the northern hemisphere on November 20, 1969. The electric field reversal, ~50 mv m^{-1}, at 00h 27m 45s to 00h 28m 05s UT occurs within the most energetic of the inverted V bands.

sentation, orbit 5696, crossed the northern auroral zone in the local evening sector at 18.8 hours MLT. A color-coded energy-time spectrogram of the precipitated (pitch angle $\alpha = 0°$) electron intensities for this pass is shown in Plate 1. The ordinate of this spectrogram is electron energy in units of electron volts, and the abscissa is universal time [*Frank and Ackerson*, 1971]. The detector response is color-coded from blue to red (low- to high-detector responses) according to the log scale shown on the right side of the spectrogram. During this pass, two intense inverted V electron precipitation events are observed at about 00h 27m 10s to 00h 28m 30s UT. The average electron energy for the most energetic of these events extends up to several kev, and substantial electron intensities can be seen at energies up to 15 kev, which is the upper limit for the spectrogram. The precipitated electron energy fluxes during this pass are shown in Figure 6. The inverted V events are located poleward of the electron ($E > 45$ kev) trapping boundary, which is at 00h 27m 20s (±10 sec) UT. The region of lower

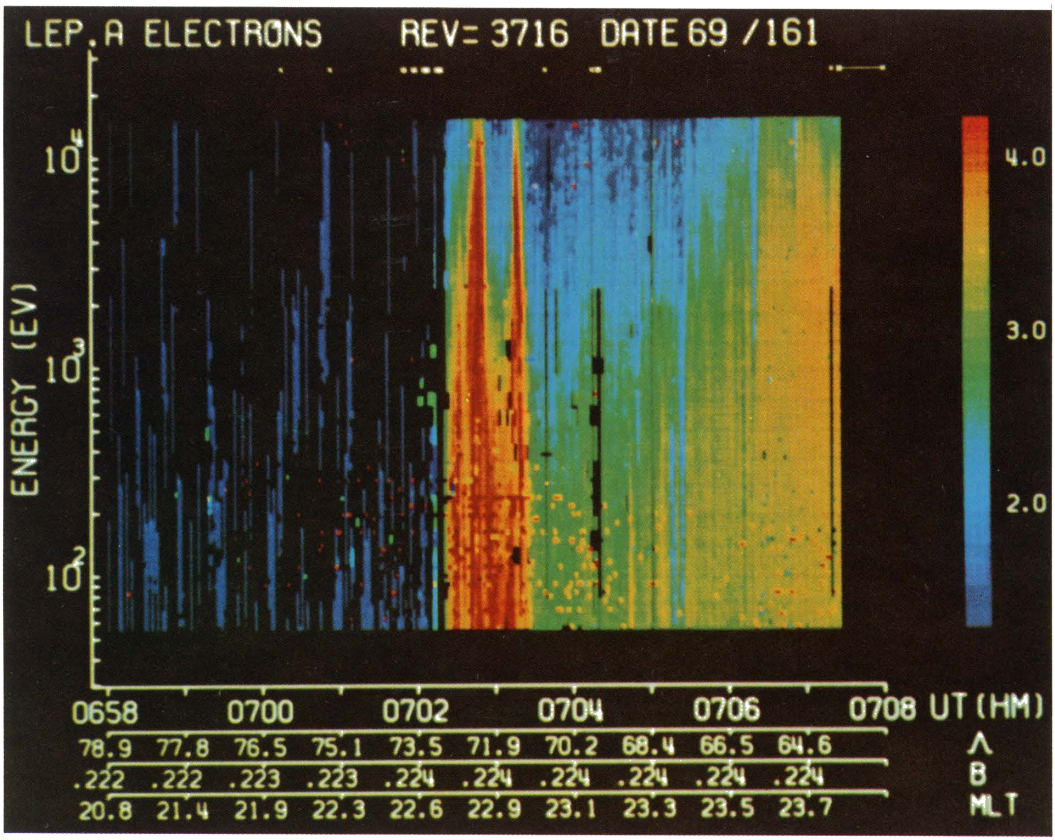

Plate 2. Energy-time spectrogram of the precipitated electron intensities observed for a northern hemisphere pass over the auroral zone at about 23.0 hours MLT. Several inverted V electron precipitation bands are evident at 07h 02m 20s to 07h 03m 25s UT. The plasma sheet extends from about 07h 03m 25s UT to the end of the pass at 07h 07m 25s UT.

electron intensities positioned equatorward of the electron ($E > 45$ kev) trapping boundary, spanning the period 00h 26m 20s to 00h 27m 10s UT, and in the energy range extending up to several kev is identified as the low-altitude signature of the plasma sheet in the local evening sector [*Ackerson and Frank*, 1972]. The abrupt decrease of the precipitated electron intensities to near background levels at 00h 27m 35s (±5 sec) UT evident in both Plate 1 and Figure 6 is not due to a loss of data or any other known instrumental effect. These 'holes' in the precipitated electron intensities are occasionally encountered near the inverted V events and are believed to be regions where the high intensities of upgoing low-energy (~100 ev) electrons reported by *Gurnett and Frank* [1972] occur.

The electric fields for this pass are shown in Figure 6. A highly structured electric field reversal is evident at 00h 27m 45s to 00h 28m 05s UT as the spacecraft passes through the major electron precipitation band. Although the relative variations in the electric field are accurate to about ±10 mv m^{-1}, the spacecraft orientation on this pass cannot be determined with sufficient accuracy (owing to the short duration of the pass) to give the $\mathbf{V}_s \times \mathbf{B}$ field to this accuracy. The $\mathbf{V}_s \times \mathbf{B}$ field is therefore not shown in Figure 6. Our best estimates are that the $\mathbf{V}_s \times \mathbf{B}$ field component along the antenna axis is about −75 mv m^{-1} in the vicinity of the reversal. As is indicated in Figure 6, the electric antenna is oriented to detect the SE-NW component of the electric field during this pass. The overall change in the electric field at the position of the reversal

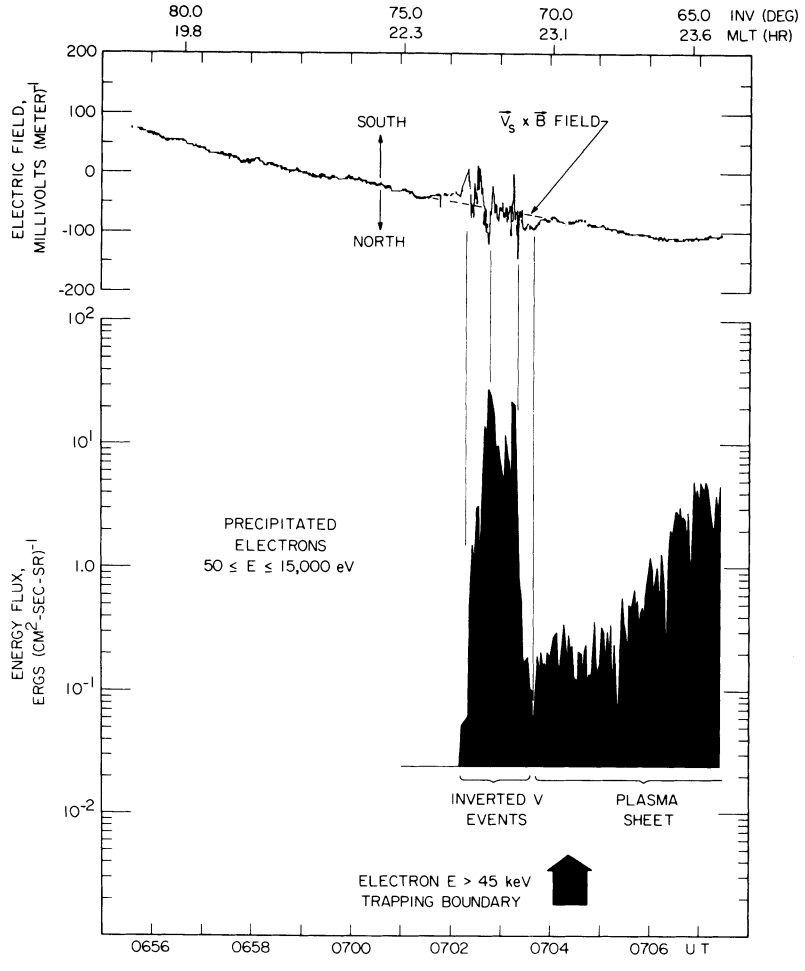

Fig. 7. The electric fields and precipitated electron energy fluxes corresponding to the energy-time spectrogram of Plate 2 for orbit 3716 over the northern hemisphere on June 10, 1969. Note the large, ~50 mv m^{-1}, irregular electric field variations associated with the inverted V events and the absence of any comparable fluctuations within the plasma sheet region.

(from NW to SE with increasing latitude) is consistent with the convection velocity directions usually observed at this local time (i.e., sunward flow equatorward of the electric field reversal and antisunward flow poleward of the electric field reversal). It is evident from Figure 6 that the reversal in the electric field directions, at about 00h 27m 45s to 00h 28m 05s UT, occurs coincident with the location of the most intense inverted V event encountered during this pass. Many large impulsive fluctuations in the electric field are observed within and near the electric field reversal. As is shown by the vertical guide lines in Figure 6, many of these impulsive variations appear to be associated with distinct features, boundaries, and maximums of the precipitated electron energy fluxes.

Orbit 3716. The second pass selected for presentation, orbit 3716, occurs later in the local evening, at a local time of about 23.0 hours MLT. The energy-time spectrogram for the precipitated electron intensities during this pass is shown in Plate 2. Several intense inverted V electron precipitation events appear in the energy-time spectrogram at 07h 02m 20s to 07h 03m 25s UT. The two most energetic of these events have average electron energies of several kev and substantial intensities at ener-

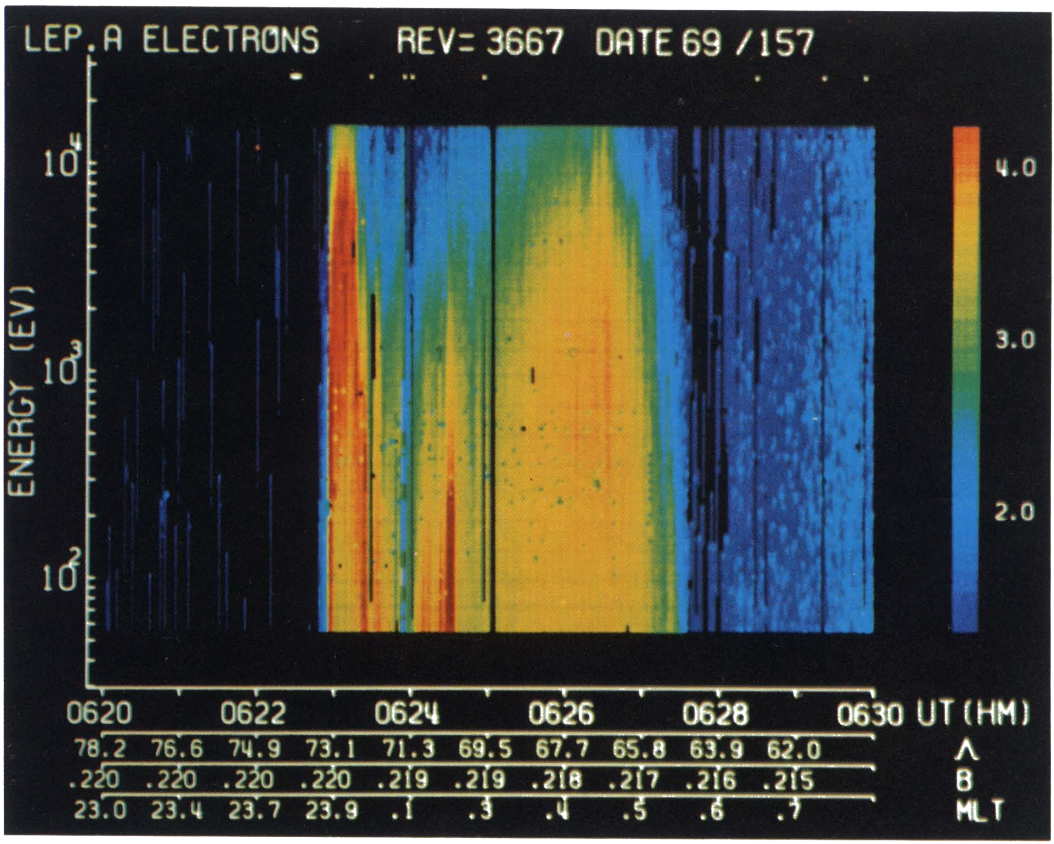

Plate 3. Energy-time spectrogram of the precipitated electron intensities observed for a northern hemisphere pass over the auroral zone at about 24.00 hours MLT. Several inverted V events are evident at 06h 22m 55s to 06h 24m 45s UT. The plasma sheet is encountered at 06h 24m 45s to 06h 27m 30s UT.

gies of >15 kev. At energies below about 1 kev the electron precipitation is a relatively continuous band at 07h 02m 20s to 07h 03m 25s UT. As is shown in Figure 7, peak precipitation energy fluxes for these inverted V events are about 20–30 ergs $(cm^2\ sec\ ster)^{-1}$. The inverted V electron precipitation events are again located poleward of the electron ($E > 45$ kev) trapping boundary (see Figure 7).

The broad zone of lower electron intensities near and equatorward of the electron ($E > 45$ kev) trapping boundary, at about 07h 03m 25s UT to the end of the pass at 07h 07m 25s UT, is identified as the low-altitude signature of the plasma sheet via the energy spectrums and intensities of these precipitated electrons. As is seen from Figure 7, the peak precipitated energy fluxes of the inverted V events are greater than the precipitated energy fluxes of the plasma sheet electrons by a factor of 5 or more.

Reference to Figure 7 shows that the primary convection electric fields observed on this pass are confined to the region near the inverted V events. Because of the absence of sunlight shadowing errors and the slow rotation of the spacecraft the $\mathbf{V}_s \times \mathbf{B}$ field can be determined with excellent accuracy, ± 10 mv m^{-1}, on this pass. No single well-defined electric field reversal is evident for this pass. However, a persistently southward electric field component of up to ~ 50 mv m^{-1} is observed from about 07h 01m 30s to 07h 02m 00s UT, just poleward of the inverted V events, and a northward electric field component of up to ~ 30 mv m^{-1} is observed at 07h 03m 25s to 07h 03m 50s, just equatorward of the inverted V events. These electric field

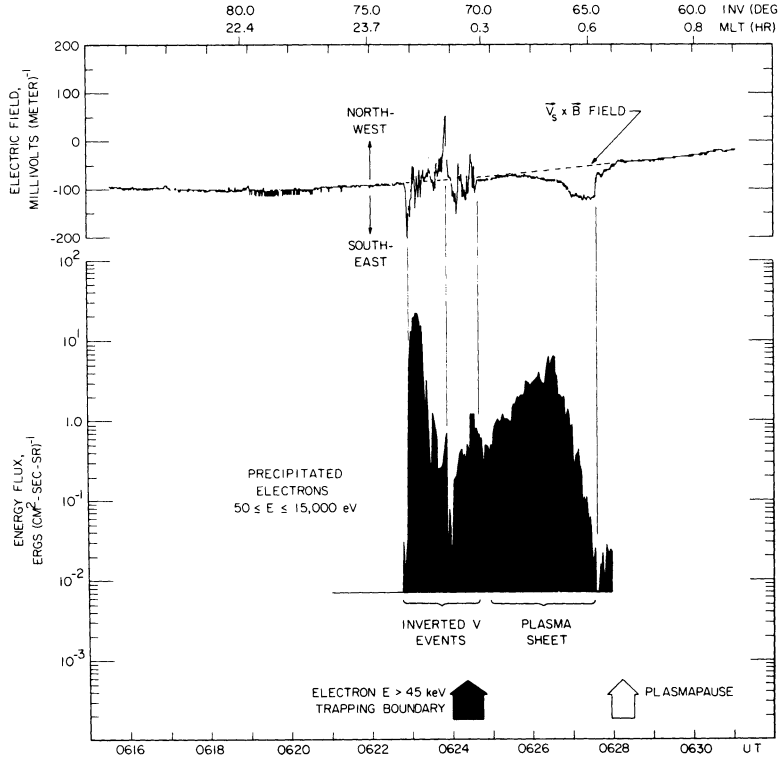

Fig. 8. The electric field and precipitated electron energy fluxes corresponding to the energy-time spectrogram of Plate 3 for orbit 3667 over the northern hemisphere on June 6, 1969. Note the large irregular electric field fluctuations associated with the inverted V events and the large, ~65 mv m^{-1}, electric fields near the equatorward boundary of the plasma sheet. The equatorward termination of this convection zone is coincident with the plasmapause location as determined with simultaneous VLF electric field measurements.

directions correspond to eastward convection on the poleward side of the inverted V events and westward convection equatorward of the inverted V events. These convection directions are again consistent with the plasma flow directions usually observed on either side of an electric field reversal in the local evening region. We therefore identify the region of the inverted V events in Figure 7 as being coincident with a small rather poorly defined electric field reversal.

In the region of the electric field reversal, many large irregular fluctuations in the electric field, of the order of ±50 mv m^{-1}, are observed with time scales of a few seconds. In several cases, these irregular variations are closely related to well-defined boundaries of the inverted V electron precipitation bands. For example, the inverted V event at 07h 03m 15s UT is bounded by a brief (1 sec) 50-mv m^{-1} southward spike in the electric field at the poleward boundary of the event (07h 03m 10s UT) and by a similar northward spike at the equatorward boundary (07h 03m 20s UT). In this case the inverted V band occurs in a region with a large latitudinal gradient in the N-S electric field (corresponding to a shear in the E-W plasma flow) between these two spikes. The inverted V event at 07h 02m 50s UT also appears to be associated with a large latitudinal gradient in the N-S electric field, although the detailed association is not as discernible in this case. No convection electric fields are detectable in the plasma sheet region during this pass.

Orbit 3667. The third pass selected, orbit 3667, is positioned near local midnight. The energy-time spectrogram for the precipitated electron intensities during this pass is shown in Plate 3. A notably intense inverted V electron

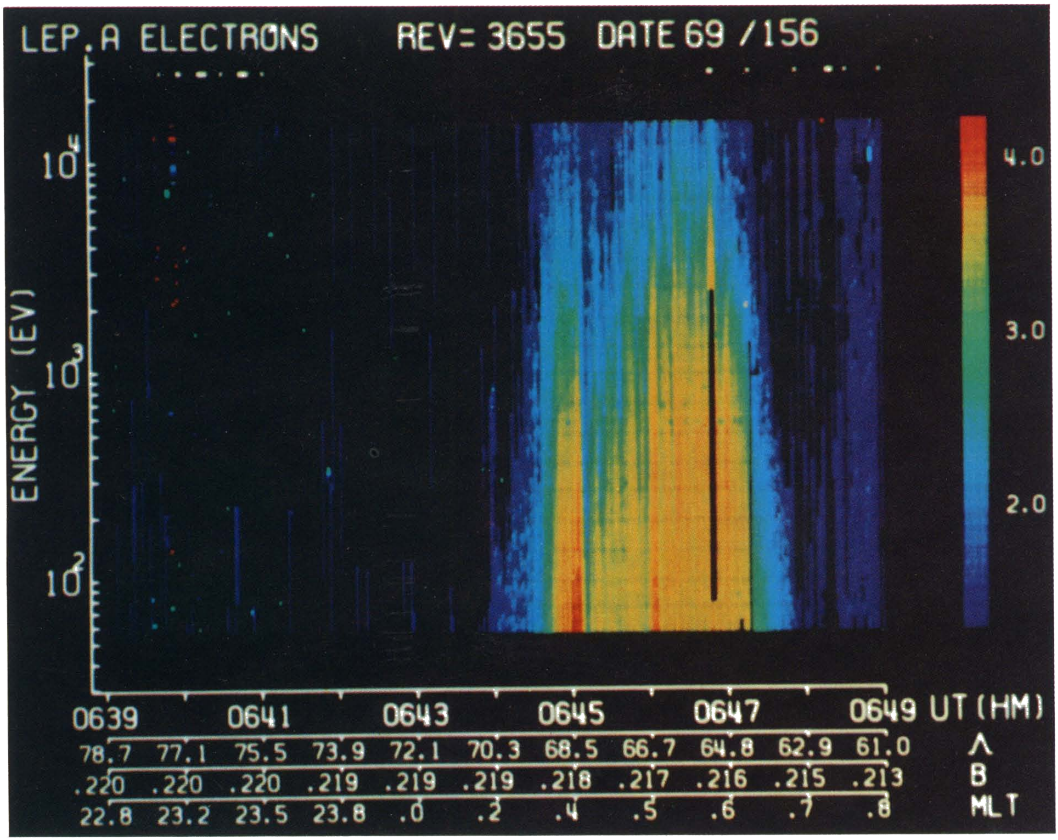

Plate 4. Energy-time spectrogram of the precipitated electron intensities observed for a northern hemisphere pass over the auroral zone at about 0.5 hours MLT. A moderate inverted V event is observed at 06h 44m 40s to 06h 45m 15s UT and the plasma sheet extends from 06h 45m 15s to 06h 47m 30s UT.

precipitation event is evident in this spectrogram at 06h 22m 55s to 06h 23m 25s UT. Several less distinct inverted V bands with maximum energies of a few kev are also evident at 06h 23m 25s to 06h 24m 45s UT. As is shown in Figure 8, the electron energy flux for the most intense of these events is about 20 ergs $(cm^2\ sec\ ster)^{-1}$. As usual, the inverted V events are located poleward of the electron ($E > 45$ kev) trapping boundary.

The region of lower electron intensities encountered at 06h 24m 45s to 06h 27m 30s UT, equatorward of the electron ($E > 45$ kev) trapping boundary, is again identified as the plasma sheet. The maximum precipitated electron energy flux in the plasma sheet region is about 6 ergs $(cm^2\ sec\ ster)^{-1}$, a flux larger than that in the previous two plasma sheet observations but, again, significantly smaller than the peak precipitated energy flux in the inverted V band. The equatorward termination of the plasma sheet can be readily seen at 06h 27m 30s UT in both Plate 3 and Figure 8.

The electric fields for this pass are shown in Figure 8. Again the electric field can be determined with an accuracy of ± 10 mv m^{-1} or better. As is seen in Figure 8, measurable convection electric fields are detected within both the inverted V and plasma sheet zones during this pass. The electric field in the inverted V region is again characterized by large, ~ 50 mv m^{-1}, irregular fluctuations with time scales of a few seconds. The most striking features of these electric field variations are the ~ 125-mv m^{-1} spike in the southeastward electric field component at 06h 22m 55s UT and a very similar but oppositely directed (northwestward) spike at 06h 23m 50s UT. The onset

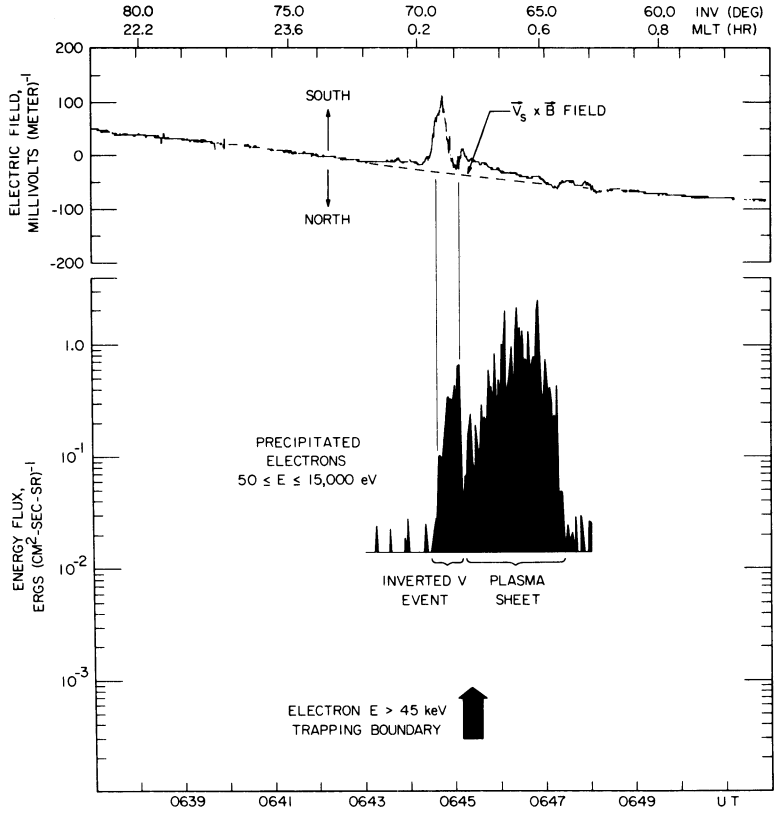

Fig. 9. The electric field and precipitated electron energy fluxes corresponding to the energy-time spectrogram of Plate 4 for orbit 3655 over the northern hemisphere on June 5, 1969.

of the first southeastward spike is coincident, within the accuracy of the determination, with the poleward boundary of the major inverted V event. As is shown by the vertical guide lines in Figure 8, the second northwestward spike is coincident with the equatorward boundary of this inverted V band. The electric field between these two spikes is very irregular, but it does appear to have an overall gradient from SE to NW as the spacecraft moves equatorward. Despite the remarkable latitudinal symmetry of the electric field associated with these two spikes the inverted V event is not located symmetrically with respect to the electric field variations. As is shown in Figure 8, the maximum energy fluxes for the inverted V event are located poleward of the midpoint between these two spikes. Further equatorward, at 06h 23m 50s to about 06h 24m 40s UT, more irregular fluctuations in the electric field of lesser amplitudes are observed and are associated with relatively moderate electron precipitation events.

When the spacecraft enters the plasma sheet at about 06h 24m 45s UT, the large irregular electric field fluctuations characteristic of the inverted V electron bands abruptly terminate, and the electric field variations become relatively smooth. Within this plasma sheet region the convection electric field is <10 mv m^{-1} near the poleward boundary, but it increases to approximately 65 mv m^{-1} near the equatorward boundary of the plasma sheet. This electric field component near the equatorward boundary of the plasma sheet is in the southeastward direction and corresponds to a northeastward convection velocity component of about 2.9 km sec^{-1}. At the equatorward boundary of the plasma sheet the convection electric field abruptly decreases to zero, as is shown by the vertical guide line at 06h 27m 35s UT in Figure 8. The plasmapause is located at 06h 28m 15s ($\pm$30 sec) UT,

nearly coincident with the equatorward boundary of the plasma sheet. The plasmapause location is identified here by a break-up of the lower hybrid resonance noise band, known to occur at the plasmapause boundary [*Carpenter et al.*, 1968], and by an abrupt increase in electron densities simultaneously monitored with the Air Force Cambridge Research Laboratory electron density instrument on Injun 5. A very similar example of large convection electric fields near the equatorward termination of the plasma sheet is found in Figure 1 at 09h 03m 00s to 09h 05m 00s UT.

Orbit 3655. The fourth pass selected for discussion, orbit 3655, traverses the auroral zone at approximately 0.5 hours MLT and has been chosen to further illustrate phenomena within the midnight sector. The energy-time spectrogram for the precipitated electron intensities during this pass is shown in Plate 4. The electron ($E > 45$ kev) trapping boundary is located at 06h 45m 20s (± 10 sec) UT as is shown in Figure 9. On this pass a single inverted V precipitation band with moderate intensities is located just poleward of the trapping boundary, at 06h 44m 40s to 06h 45m 15s UT. The region equatorward of the trapping boundary, at 06h 45m 15s to 06h 47m 30s UT, is again identified as the plasma sheet from the characteristic spectrums and intensities of the plasma sheet electrons and their location equatorward of the trapping boundary. For this example the maximum precipitated electron energy flux in the inverted V band is less than that within the plasma sheet region, as is typical of the auroral charged-particle precipitation observed in the local postmidnight and dawn sectors [*Frank and Ackerson*, 1972].

As can be seen readily from Figure 9, the electron energy fluxes in the plasma sheet have quasi-periodic pulsations with periods of about 10 sec. These pulsations are also seen in the spectrogram of Plate 4, especially at energies above about 1 kev, and in the electron ($E > 45$ kev) intensities (not shown here). *Frank and Ackerson* [1973] have determined the length of the magnetic field line from the spacecraft to the corresponding mirror point in the opposite hemisphere during this pass from the echo time of identifiable packets of electrons with $E > 45$ kev associated with these pulsations. Such observations showed that the magnetic field line length, from mirror point to conjugate mirror point, varied from about 25 R_E at 06h 46m 44s UT to 50 R_E at 06h 46m 23s UT for the most intense segment of electron precipitation from the plasma sheet. The corresponding geocentric radial distances at the magnetic equator for these field lines are 10 and 20 R_E, respectively, in the dipole approximation. *Frank and Ackerson* [1973] present substantial evidences that pulsating auroras (P_1) can be attributed to such fluctuations of plasma sheet energy fluxes as those shown in Figure 9.

The electric fields for this pass are shown in Figure 9. Significant deviations of the measured electric field from the $\mathbf{V}_s \times \mathbf{B}$ field are evident throughout the inverted V and plasma sheet zones. In contrast with the three previous examples the electric field variations are relatively smooth with only small, <10 mv m^{-1}, fluctuations on a time scale of a few seconds or less. The most prominent electric field effect for this pass is the large southward electric field component detected at about 06h 44m 30s to 06h 44m 55s UT. This electric field corresponds to a zone of eastward convection and is associated with the moderate inverted V event positioned just poleward of the trapping boundary. As for previous examples the spatial features of the electric fields and of the inverted V event are not exactly congruent. The maximum in the convection electric field is positioned slightly poleward of the most energetic part of the inverted V event. However, the inverted V band is again located within a region that has a large latitudinal gradient in the N-S electric field. In the plasma sheet a small, ~ 30 mv m^{-1}, southward electric field is observed, which decreases to zero at the equatorward boundary of the plasma sheet at 06h 47m 20s. The electric field variations within the plasma sheet are quite different from those observed for orbits 7476 (Figure 1) and 3667 (Figure 8) for which the electric fields reach a maximum near the equatorward boundary of the plasma sheet. No fluctuations of the electric field are found that can be associated with the pulsations of plasma sheet energy fluxes.

DISCUSSION AND INTERPRETATION OF LOCAL EVENING OBSERVATIONS

In the dayside polar cusp at low altitudes the intense low-energy (~ 100 ev) inverted V electron precipitation bands are positioned at the

electric field reversal and the electron ($E > 45$ kev) trapping boundary. This general relationship is also observed frequently for the more energetic (1–10 kev) inverted V electron precipitation events at local evening (see Figure 6, for example). The inverted V bands are broader in these later local time sectors and are located typically in a region adjacent to and poleward of the trapping boundary. However, these bands have also been observed at latitudes substantially above the trapping boundary [cf. *Frank and Ackerson*, 1972]. At still later local times, in the late-evening and premidnight sectors, the electric field reversals are smaller and less distinct, and, in many cases, a single well-defined electric field reversal cannot be identified (see Figures 7, 8, and 9 as examples). When a clearly defined electric field reversal can be identified, an inverted V electron precipitation event is usually positioned at the electric field reversal. Although the dominant precipitated electron energy fluxes in the local evening are due to the inverted V bands, smaller but still significant electron precipitation is also found in the plasma sheet region equatorward of the electric field reversal. From the standpoint of comparing these results with ground-based observations, it is important to note that, although the most intense auroral arcs are usually produced by the inverted V events at the electric field reversal, visible auroral emissions can also be expected from the plasma sheet electrons precipitated in the region of generally sunward convection equatorward of the electric field reversal, particularly during the expansive phase of a polar magnetic substorm.

For all cases investigated here in the local afternoon and evening sectors the inverted V electron precipitation events are found to be associated with large, typically >30 mv m^{-1}, irregular electric field fluctuations with time scales of a few seconds or less. These electric field fluctuations are normally confined to the immediate vicinity of the inverted V events, as in Figures 7 and 8. In many cases, these irregular fluctuations provide such a distinctive 'signature' that the location of the inverted V events could be predicted with good reliability from the electric field measurements alone without prior reference to the plasma observations. Often these electric field variations appear to comprise one or more pairs of oppositely directed 'spikes,' of a few seconds duration or less, each of which is usually identified with distinct boundaries of the electron precipitation region (see Figure 8 at 06h 22m 55s and 06h 23m 50s UT, for example). The abrupt changes in the electric field at the boundaries of the precipitation region may correspond to the abrupt rotation in the electric field direction observed on rocket flights [*Mozer and Fahleson*, 1970; *Choy et al.*, 1971] near the boundaries of an auroral arc. It is of interest to note that these oppositely directed spikes in the N-S component of the electric field, as in Figure 7 at 07h 02m 35s to 07h 02m 50s UT, correspond to a decrease in the electrostatic potential within the inverted V region. The inverted V events, however, are usually not located symmetrically relative to the spatial configuration of these oppositely directed electric fields. In most cases the energetic part of the inverted V event occurs where a large latitudinal gradient exists in the N-S electric field component (see Figure 9 at 06h 44m 45s UT, for example). Within the energetic part of the inverted V event the electric field can be quite large, >50 mv m^{-1} (see Figure 7 at 07h 02m 50s UT, for example), in contrast with various rocket measurements of electric fields at lower altitudes [*Aggson*, 1969; *Potter*, 1970], which indicate that the electric field is small, <10 mv m^{-1}, within an auroral arc. These contrasting results at different altitudes could be taken as evidence for an electric field component parallel to the geomagnetic field. However, other rocket measurements [*Mozer and Fahleson*, 1970] have shown that larger, ~ 30 mv m^{-1}, electric fields are also observed in auroral arcs. Because of the relatively few rocket measurements of electric fields within auroral arcs in the ionosphere and the uncertainty as to whether these flights pass through inverted V events comparable to those detected by Injun 5, we feel that no firm conclusions can be drawn about the presence of electric fields directed parallel to the geomagnetic field from the body of observations discussed above.

In the plasma sheet, equatorward of the electron ($E > 45$ kev) trapping boundary, the electric field variations are quite different from those in the inverted V electron precipitation bands. The electric field in the plasma sheet is usually relatively smooth on a time scale of tens of seconds (or a horizontal distance scale

of hundreds of kilometers) or less with no evidence of the large-amplitude electric field fluctuations such as those encountered in the inverted V region (compare these two regions in Figure 8, for example). In the local dawn and dusk sectors the convection velocities in the plasma sheet are generally sunward, since the plasma is located on closed geomagnetic field lines equatorward of the electric field reversal [*Frank and Gurnett*, 1971]. In the local midnight sector the convection electric field is highly variable with marked changes in both magnitude and direction from pass to pass. In Figure 7, for example, no convection electric field is detectable within the plasma sheet during this pass. The plasma sheet observations of Figures 1 and 8, on the other hand, are characterized by relatively large convection velocities near the equatorward boundary of the plasma sheet. However, the directions of the convection velocity components detected in the plasma sheet are different for these two cases (westward in Figure 1 and northeastward in Figure 8). The variability in the E-W direction of the convection velocity near local midnight is probably due to the fluctuations in the E-W location of the stagnation point for the generally sunward flow of plasma from the geomagnetic tail. The large convection velocities, $\sim$3 km sec^{-1}, at the equatorward boundary of the plasma sheet may mean that convection electric fields are more important than they were previously thought to be for the transport, loss, and de-energization of plasma sheet charged particles penetrating into this region of the magnetosphere (see discussions by *Vasyliunas* [1968] and *Kennel* [1969]).

OBSERVATIONS DURING A POLAR MAGNETIC SUBSTORM

In this section we present a series of low-altitude observations during a polar magnetic substorm. The substorm of interest here occurred at 1530–1900 UT on February 24, 1970. Several factors contribute to making the satellite measurements during this event particularly useful for investigating electric field and plasma phenomena associated with a substorm. First, the magnetic signature of this substorm is exceptionally clear. The magnetic disturbances during this storm have a well-defined onset and are preceded by a period of several hours during which no significant magnetic activity is observed. Second, essentially continuous worldwide observations are available in the dawn-dusk meridional plane both before and during this event. Third, the rotation rate, orientation, and altitude of the spacecraft are such that the ($\sim$N-S) convection electric field can be determined with an accuracy of better than $\pm$10 mv m^{-1} over both the northern and southern hemispheres during the substorm.

Superposed H traces from the magnetograms of a series of selected auroral zone observatories are shown in Figure 10 for the period of this polar magnetic substorm (S.-I. Akasofu, private communication, 1972). The difference between the upper trace and the lower trace of the envelope is the auroral electrojet activity index *AE*. The onset of the substorm is clearly signaled by the abrupt increase in the *AE* index at about 1530 UT. Following the onset of the substorm a negative bay of about 500 γ is observed at numerous auroral zone magnetic observatories in the local evening and midnight sectors. The magnetic disturbances associated with this substorm reach a maximum at 1600–1630 UT and recover to the prestorm values at about 1900 UT.

The convection velocity components for three consecutive polar passes during the initial phases of the substorm are shown in Figure 11. The northern hemisphere polar pass of orbit 6871 occurs well before the onset time of the substorm. The convection velocities during this pass are generally small except for a small region at local morning at about 80° invariant latitude. The next polar pass is over the southern hemisphere on orbit 6871. This pass is nearly coincident with the onset of the substorm (see Fig-

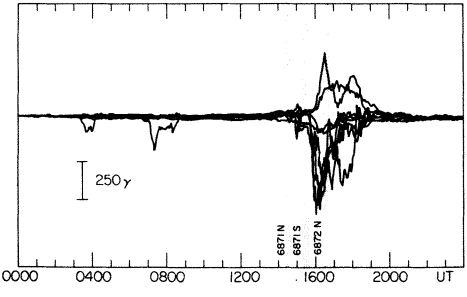

Fig. 10. Superposed H traces from the magnetograms of a series of selected auroral zone observatories during the polar magnetic substorm of February 24, 1970.

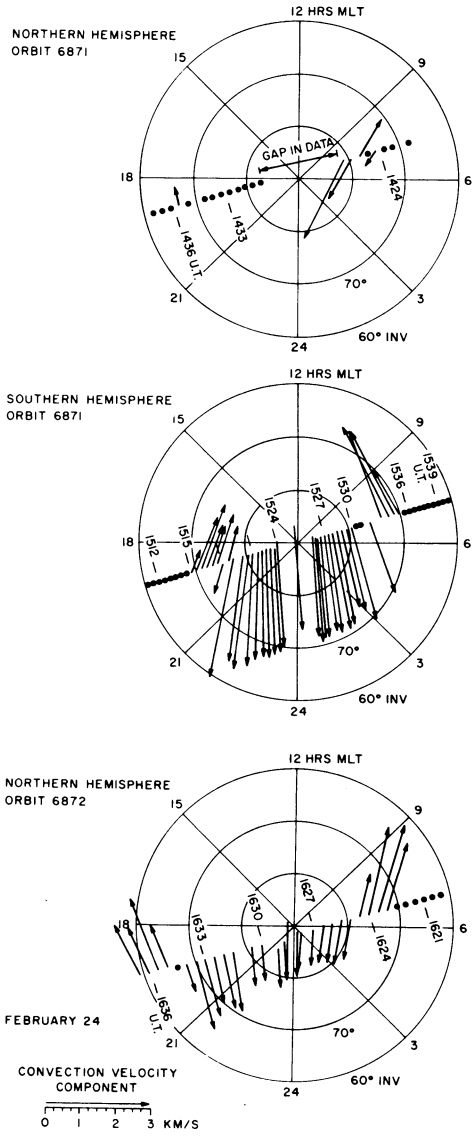

Fig. 11. A polar plot of the direction and magnitude of the convection velocity components detected during the magnetic substorm of February 24, 1970. The time periods of these polar passes are the shaded areas in Figure 10.

ure 10). Very large convection velocities, $\gtrsim$3 km sec^{-1}, are detected over the polar region during this pass. The plasma convection during this pass comprises a large zone of antisunward flow over the polar cap and adjacent zones of sunward flow at lower latitudes in the local morning and evening sectors. These zones of sunward and antisunward flow are separated by electric field reversals at about 15h 19m 00s and 15h 33m 00s UT. The antisunward convection velocities over the polar cap for this pass are unusually large and are not commonly encountered with Injun 5. However, similar cases with nearly uniform antisunward convection velocities over the polar cap have been reported previously [e.g., *Cauffman and Gurnett*, 1971, Figure 7]. The next polar pass is over the northern hemisphere on orbit 6872. This pass occurs about 1 hour after the onset of the substorm and shortly after the time of maximum magnetic disturbance. The convection velocities during this pass are again in the antisunward direction over the polar cap and in the sunward direction at lower latitudes. These zones of oppositely directed plasma flow are separated by electric field reversals located at about 16h 24m 30s and 16h 34m 00s UT. The convection velocities, $\sim$1.5–2.0 km sec^{-1}, are smaller and less uniform over the polar cap relative to those of the preceding pass over the southern hemisphere. The equatorward boundary of the sunward convection zone at local evening has also shifted from $\sim$70° to $\sim$59° invariant latitude during the time interval, $\sim$75 min, between the southern hemisphere pass of orbit 6871 and the northern hemisphere pass of orbit 6872 (see Figures 12 and 13). The electric fields for subsequent passes during the recovery phase of the substorm display a general trend toward smaller convection velocities, $\lesssim$0.75 km sec^{-1} by 1900 UT, with less uniformity in the zone of antisunward plasma flow over the polar cap.

The electric field and charged-particle observations for the southern hemisphere pass of orbit 6871 near the onset of the substorm are shown in Figure 12. The electric field reversals separating the regions of sunward and antisunward plasma flow are evident in Figure 12 at about 15h 19m 00s and 15h 33m 00s UT. The electron ($E > 45$ kev) trapping boundary at local evening, shown by the vertical dashed line at 15h 16m 00s UT, is located within the zone of sunward convection several degrees equatorward of the electric field reversal. This relationship is very unusual, since, as was shown previously by *Frank and Gurnett* [1971], the electron ($E >$ 45 kev) trapping boundary is typically positioned coincident with the electric field reversal, to within the accuracy of the determination. The

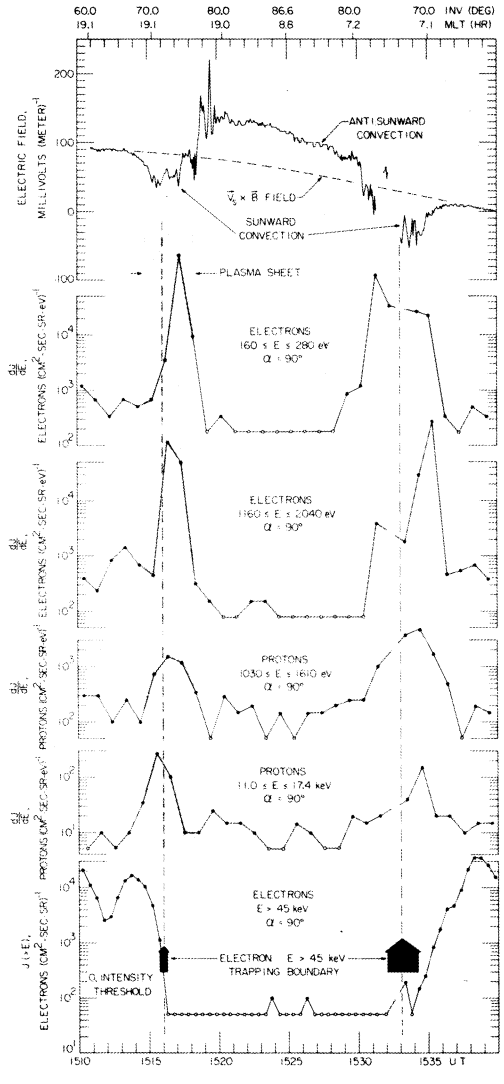

Fig. 12. The simultaneous electric field and charged-particle measurements during the southern hemisphere polar pass of orbit 6871 on February 24, 1970, approximately 10–15 min before the onset of the expansive phase of the substorm. Shaded area indicates a region of enhanced low-energy electron and proton intensities.

electron ($E > 45$ kev) trapping boundary in this case clearly does not coincide with the boundary between open and closed magnetic field lines, since the sunward plasma flow equatorward of the electric field reversal occurs on closed magnetic field lines [*Frank and Gurnett*, 1971]. In fact, since the most probable source of magnetospheric plasmas in these regions is the magnetosheath, which is known to be relatively void of these more energetic electron intensities, there is no compelling reason to believe that all closed field lines must always be populated with measurable intensities of these energetic electrons, particularly with respect to

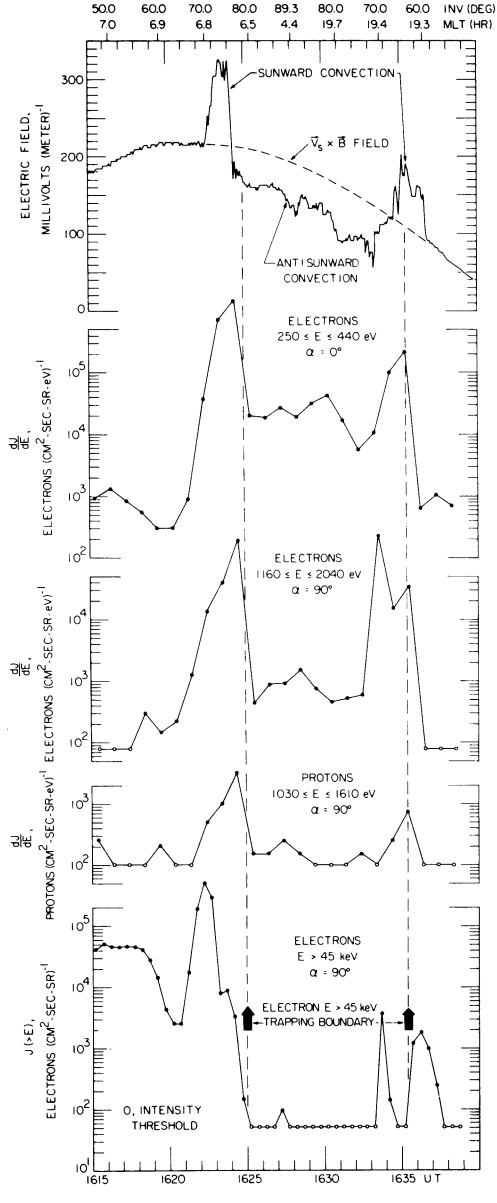

Fig. 13. Simultaneous electric field and charged-particle measurements for the northern hemisphere polar pass of orbit 6872 on February 24, 1970, shortly after the expansive phase of the substorm.

regions of newly injected plasma within the plasma sheet. This sunward plasma flow in the local evening sector is also associated with a region of enhanced low-energy electron and proton intensities shown in Figure 12. From the relatively soft energy spectrums and overall intensities of these particles and their location on closed magnetic field lines the region encountered at 1516–1518 UT is observationally identified with the plasma sheet adjacent to the downstream magnetosheath along the evening flanks of the magnetosphere [cf. *Frank and Gurnett*, 1971, Figure 7]. The enhanced intensities of lower-energy electrons and of $1030 \leq E \leq 2040$ ev protons within this zone are believed to be those of magnetosheath plasma, which is being injected into the plasma sheet. The intensities of higher-energy protons ($11.0 \leq E \leq 17.4$ kev) at 1513–1516 UT are to be identified as the signature of the earthward extension of the plasma sheet, the extraterrestrial ring current. The latitudinal distribution of the plasma sheet electron intensities, the location of the electron ($E > 45$ kev) trapping boundary, and the penetration of the ring current protons to L values lower than those of the plasma sheet electrons are in substantial agreement with the spatial structure of the near-earth plasma sheet reported by *Frank* [1971*c*] at similar local times with high-altitude measurements near the magnetic equatorial plane.

The electric field and charged-particle observations at approximately 1 hour later, during the northern hemisphere pass of orbit 6872, are shown in Figure 13. The electric field reversals separating the regions of sunward and antisunward plasma flow are well defined and located at 16h 24m 30s and 16h 34m 00s UT. The positions of the two electron ($E > 45$ kev) trapping boundaries are shown by the vertical dashed lines in Figure 13. In contrast with the preceding pass, the electric field reversal and the trapping boundary in the local evening sector of this pass are located more nearly coincident, within $\sim 2°$ invariant latitude of each other. However, the electron ($E > 45$ kev) intensities are seen to have changed severely within the outer radiation zone during the time interval between these two passes. By comparing Figures 12 and 13 it can be seen that the electron ($E > 45$ kev) intensities decreased by approximately 1 order of magnitude at local evening and increased by approximately 1 order of magnitude at local morning. *Craven* [1966] has reported similar observations of abrupt depletions of the outer radiation zone electron intensities at low altitudes during magnetic storms. Since no similarly spectacular depletion of the outer zone electron intensities has been reported for measurements near the magnetic equatorial plane to our knowledge, it is presumed that this 'depletion' effect observed at low altitudes involves principally only electrons with pitch angles within and near the loss cone.

The abrupt increase of electron ($E > 45$ kev and $1160 \leq E \leq 2040$ ev) intensities at 16h 33m 45s (± 15 sec) UT, poleward of the trapping boundary in the local evening sector, is attributed to an energetic inverted V electron precipitation band [cf. *Frank and Ackerson*, 1972]. Although the detailed inverted V energy-time structure cannot be resolved with these low bit rate observations, several characteristic features allow us to identify this intensity increase as an inverted V type event. These characteristics include the location of the event poleward of the trapping boundary, the electron energy spectrum and intensities, and the angular distribution of the electron intensities. Note that this inverted V event is also associated with an abrupt change in the ($\sim$N-S) electric field at about 16h 33m 30s UT, a behavior similar to that in the electric field of orbit 5696 displayed in Figure 6.

As is shown by the electron intensities at $250 \leq E \leq 440$ ev and $1160 \leq E \leq 2040$ ev of Figure 13, enhanced intensities of low-energy (100 ev to 1 kev) electrons are observed throughout the region of antisunward convection at 16h 24m 30s to 16h 34m 00s UT. The electron intensities are nearly uniform at intensity levels that are greater by more than an order of magnitude than the threshold intensity for the detector in these energy ranges over the polar caps. These electron intensities are anisotropic, the intensities at pitch angles $\alpha = 90°$ being factors of ~ 5 less than those at $\alpha = 0°$. Normally, the electron intensities observed over the polar caps are at or near the intensity threshold of the detector for these energy ranges. For example, no comparable electron intensities are observed over the southern polar cap region during the pass shown in Figure 12 or during the preceding northern hemisphere pass 2 hours

earlier. Measurements for the remaining polar passes during the substorm recovery show that the enhanced polar cap electron intensities continue to be present for a period of about 2 hours over the northern polar cap at somewhat lesser intensities. However, comparable electron intensities are not observed over the southern polar cap for any pass during this event. Thus a pronounced N-S asymmetry appears to exist for the intensities of this low-energy polar cap electron precipitation. This asymmetry for the polar cap intensities during substorm and quiescent periods will be discussed more thoroughly in a future report.

DISCUSSION AND INTERPRETATION OF THE SUBSTORM OBSERVATIONS DURING FEBRUARY 24, 1970

The simultaneous electric field and plasma measurements reported here for the polar magnetic substorm of February 24, 1970, delineate several important new features of magnetospheric electric fields and their relationship to the dynamical processes occurring during a polar magnetic substorm. As was discussed by *Rostoker* [1972], the development of a substorm may be described in terms of three basic phases: the growth phase, the expansive phase, and the decay phase. The expansive phase is characterized by the poleward motion of visible auroral arcs [*Akasofu,* 1968] and a rapid intensification of the ionospheric current system over a period of a few minutes. The sudden onset of the magnetic perturbations evident in Figure 10 at 15h 40m 00s (±5 min) UT is identified as the start of the expansive phase of this substorm. The growth phase of a substorm is associated with a small increase in magnetic activity [*McPherron,* 1970] over a period of several tens of minutes preceding the expansive phase and is presently believed to be a signature of the injection of energy into the nightside magnetosphere. Careful inspection of the magnetograms of Figure 10 shows that the first recognizable magnetic activity associated with this storm occurred at 14h 30m 00s (±10 min) UT. Correspondingly, the relatively moderate magnetic activity at ~1430–1540 UT preceding the expansive phase is identified here with the growth phase of the substorm. The decay phase of a substorm follows the expansive phase and typically lasts for 1–2 hours. The decay phase of the February 24, 1970, substorm is readily identified in Figure 10 and spans the period ~1600–1900 UT.

An examination of the sequence of events during this particular substorm shows that the large region of antisunward plasma flow observed over the southern polar cap on orbit 6871 precedes the onset of the expansive phase of the polar magnetic substorm by 10–15 min (cf. Figures 10 and 11). Since at least an additional ~10 min is required for the convection of magnetic field lines from the dayside polar cusp region to the spacecraft, it is clear that a greatly enhanced magnetic merging rate was established at the sunlit magnetopause substantially before the expansive phase of the substorm. This increase in the merging rate at the magnetopause must have occurred not more than 1 hour before the onset of the expansive phase of the substorm, since no comparably large region of antisunward plasma flow was observed for the northern hemisphere pass of orbit 6871 1 hour earlier. However, a relatively narrow zone with convection velocities of 1–2 km sec^{-1} is detected in the local morning sector during this pass (see Figure 11). Since the growth phase of the substorm commences almost concurrently with the detection of these large convection velocities, it is believed that this zone of enhanced plasma flow in the local morning and its subsequent expansion into the large-scale flow pattern observed 1 hour later are directly associated with the growth phase of this substorm. The onset of the growth phase of this polar magnetic substorm appears to have been triggered by a notable change in the direction of the interplanetary magnetic field in the vicinity of the earth at 1420 (±10 min) UT (N. F. Ness, private communication, 1972). The direction of the interplanetary magnetic field changed from dominantly sunward to antisunward at this time. These observations of an enhanced antisunward plasma flow during the growth phase of this substorm are generally consistent with current ideas on the origin of substorms [cf. *Axford,* 1969] in which the transport and the buildup of magnetic flux in the tail of the magnetosphere precede the expansive phase of the substorm.

An estimate of the electrostatic potential over the polar regions during this substorm can be obtained from the electric field observations for

the southern hemisphere pass of orbit 6871 and the northern hemisphere pass of orbit 6872. During these traversals of the polar caps the electric antenna axis was oriented approximately parallel to the spacecraft velocity vector so that the electrostatic potential Φ can be determined by directly integrating the measured electric field E: $\Phi = -\int E\, ds$, where ds is an element of length along the satellite trajectory. The actual antenna alignment for these two passes is shown by the convection velocity directions in Figure 11 (the antenna axis is perpendicular to the arrows in this diagram). Although the antenna axis does not remain exactly parallel to the velocity vector during these passes, the error introduced by this misalignment is small, $\lesssim 10\%$, if the electric field is generally in the dawn-dusk direction, as it is expected to be here [cf. *Cauffman and Gurnett*, 1971]. The electrostatic potential differences across the regions of antisunward plasma flow over the northern and southern polar regions are computed to be about 235 and 240 kv, respectively. These potential differences are much larger than the potential differences usually encountered over the polar regions with Injun 5, which are typically of the order of 50 kv [*Cauffman and Gurnett*, 1971; *Frank and Gurnett*, 1971].

An important new relationship revealed by the charged-particle observations for this substorm is that just before the expansive phase of the substorm the electron ($E > 45$ kev) trapping boundary in the local late-evening sector was located about 5° invariant latitude equatorward of the electric field reversal (see Figure 12). Since it has been previously established that the electric field reversal and the electron ($E > 45$ kev) trapping boundary are typically coincident within observational errors [*Frank and Gurnett*, 1971], this electric field–plasma relationship must be regarded as quite unusual. We attribute the poleward movement of the electric field reversal location, relative to its usual position near the trapping boundary, as being due to the rapid reconnection of field lines in the downstream magnetosheath and creation of 'new' closed field lines in the distant plasma sheet that are not yet populated by energetic electrons with energies of $E \gtrsim 45$ kev. The observation of plasma sheet electrons and protons poleward of the trapping boundary and in the region of sunward convection (see the shaded area of Figure 12) provides substantial evidence of the increased reconnection rate and the corresponding poleward expansion of the plasma sheet as viewed at low altitudes. The subsequent relaxation of the electric field reversal location back to its usual position near the trapping boundary during the decay phase of the substorm (see Figure 13) is interpreted as being due to a decrease in the downstream reconnection rate followed by a filling up (of the region of newly created closed field lines within the plasma sheet) with energetic electrons via gradient and/or electric drifts from adjacent regions populated with such electrons or via local electron acceleration.

One further noteworthy effect encountered during this substorm is the presence of enhanced intensities of precipitated low-energy electrons over the northern polar cap during the decay phase of the substorm. Since the magnetic field lines in this region of antisunward flow must presumably pass through the magnetosheath before connecting into the solar wind, the most apparent source for these low-energy (100 ev to 1 kev) electrons is the high-latitude magnetosheath. If these precipitated electrons do originate from the magnetosheath, the question immediately arises as to why these electron intensities dramatically increased during the course of this polar magnetic substorm. The marked asymmetry in the electron precipitation over the northern and southern polar caps undoubtedly provides an important clue as to the origin of these electrons. The N-S asymmetry in the merging rates at the sunlit magnetopause at high latitudes introduced by the radial component of the solar wind magnetic field [cf. *Frank*, 1971*b*] and the asymmetry introduced by the seasonal tilt of the earth's magnetic dipole axis relative to the solar wind direction are considered the most likely asymmetries that could be responsible for the observed difference in precipitation over the northern and southern polar caps. Further examples of these electron precipitation events are being investigated to provide more information concerning the mechanisms responsible for this electron precipitation over the earth's polar caps.

Acknowledgments. We wish to thank Dr. S.-I. Akasofu for providing the magnetograms used in this study and Dr. N. F. Ness for providing the

interplanetary magnetic field measurements from the Explorer 35 satellite.

This research was supported in part by the National Aeronautics and Space Administration under contracts NAS5-10625, NAS1-8141, and NAS1-2973 and grant NGL16-001-002 and by the Office of Naval Research under contract N00014-68-A-0196-0003.

* * *

The Editor thanks R. L. Arnoldy and F. V. Coroniti for their assistance in evaluating this paper.

REFERENCES

Ackerson, K. L., and L. A. Frank, Correlated satellite measurements of low-energy electron precipitation and ground-based observations of a visible auroral arc, *J. Geophys. Res., 77,* 1128, 1972.

Aggson, T. L., Results of magnetospheric electric field measurements, paper presented at Conference on Electric Fields in the Magnetosphere, Rice University, Houston, Tex., 1969.

Akasofu, S.-I., *Polar and Magnetic Substorms,* p. 25, D. Reidel, Dordrecht, Netherlands, 1968.

Axford, W. I., Magnetospheric convection, *Rev. Geophys. Space Phys., 7,* 421, 1969.

Carpenter, D. L., F. Walker, R. E. Barrington, and D. J. McEwen, Alouette 1 and 2 observations of abrupt changes in whistler rate and of VLF noise variations at the plasmapause: A satellite ground study, *J. Geophys. Res., 73,* 2929, 1968.

Cauffman, D. P., and D. A. Gurnett, Double-probe measurements of convection electric fields with the Injun 5 satellite, *J. Geophys. Res., 76,* 6014, 1971.

Cauffman, D. P., and D. A. Gurnett, Satellite measurements of high latitude convection electric fields, *Space Sci. Rev., 13,* 369, 1972.

Choy, L. W., R. L. Arnoldy, W. Potter, P. Kinter, and L. J. Cahill, Jr., Field-aligned particle currents near an auroral arc, *J. Geophys. Res., 76,* 8279, 1971.

Craven, J. D., Temporal variations of electron intensities at low altitudes in the outer radiation zone as observed with satellite Injun 3, *J. Geophys. Res., 71,* 5643, 1966.

Dungey, J. W., Interplanetary magnetic field and the auroral zones, *Phys. Rev. Lett., 6,* 47, 1961.

Frank, L. A., Plasma in the earth's polar magnetosphere, *J. Geophys. Res., 76,* 5202, 1971*a*.

Frank, L. A., Comments on a proposed magnetospheric model, *J. Geophys. Res., 76,* 2512, 1971*b*.

Frank, L. A., Relationship of the plasma sheet, ring current, trapping boundary, and plasmapause near the magnetic equator and local midnight, *J. Geophys. Res., 76,* 2265, 1971*c*.

Frank, L. A., and K. L. Ackerson, Observations of charged-particle precipitation into the auroral zone, *J. Geophys. Res., 76,* 3612, 1971.

Frank, L. A., and K. L. Ackerson, Local time survey of plasma at low altitudes over the auroral zones, *J. Geophys. Res., 77,* 4116, 1972.

Frank, L. A., and K. L. Ackerson, Rapid temporal variations of plasma sheet electron intensities at low altitudes, submitted to *J. Geophys. Res.,* 1973.

Frank, L. A., and D. A. Gurnett, Distributions of plasmas and electric fields over the auroral zones and polar caps, *J. Geophys. Res., 76,* 6829, 1971.

Gurnett, D. A., and L. A. Frank, VLF hiss and related plasma observations in the polar magnetosphere, *J. Geophys. Res., 77,* 172, 1972.

Gurnett, D. A., G. W. Pfeiffer, R. R. Anderson, S. R. Mosier, and D. P. Cauffman, Initial observations of VLF electric and magnetic fields with the Injun 5 satellite, *J. Geophys. Res., 74,* 4631, 1969.

Haerendel, G., Electric fields and their effects in the ionosphere, in *Proceedings of the Leningrad Symposium on Solar-Terrestrial Physics,* p. 62, D. Reidel, Dordrecht, Netherlands, 1971.

Haerendel, G., and R. Lust, Electric fields in the ionosphere and magnetosphere, in *Particles and Fields in the Magnetosphere,* edited by B. M. McCormac, p. 213, D. Reidel, Dordrecht, Netherlands, 1970.

Heikkila, W. J., and J. D. Winningham, Penetration of magnetosheath plasma to low altitudes through the dayside magnetospheric cusps, *J. Geophys. Res., 76,* 883, 1971.

Heppner, J. P., Electric field variations during substorms: Ogo 6 measurements, *GSFC Rep. X-645-72-10,* 1972.

Hultqvist, B., Auroras and polar substorms: Observations and theory, *Rev. Geophys. Space Phys., 7,* 129, 1969.

Kennel, C. F., Consequences of a magnetospheric plasma, *Rev. Geophys. Space Phys., 7,* 379, 1969.

McPherron, R. L., Growth phase of magnetospheric substorms, *J. Geophys. Res., 75,* 5592, 1970.

Mozer, F. S., and U. V. Fahleson, Parallel and perpendicular electric fields in an aurora, *Planet. Space Sci., 18,* 1563, 1970.

Potter, W. E., Rocket measurements of auroral electric and magnetic fields, *J. Geophys. Res., 75,* 5415, 1970.

Rostoker, G., Polar magnetic substorms, *Rev. Geophys. Space Phys., 10,* 157, 1972.

Vasyliunas, V. M., A survey of low-energy electrons in the evening sector of the magnetosphere with Ogo 1 and Ogo 3, *J. Geophys. Res., 73,* 2839, 1968.

Wescott, E. M., J. D. Stolarik, and J. P. Heppner, Electric fields in the vicinity of auroral forms from motions of barium vapor releases, *J. Geophys. Res., 74,* 3469, 1969.

(Received April 17, 1972;
accepted July 5, 1972.)